Bio-Design and Manufacturing (2024) 7:463–475
https://doi.org/10.1007/s42242-024-00292-4

RESEARCH ARTICLE

Nacre-inspired MXene-based film for highly sensitive piezoresistive sensing over a broad sensing range

Gaofeng Wang[1] · Lingxian Meng[1] · Xinyi Ji[2] · Xuying Liu[1] · Jiajie Liang[2] · Shuiren Liu[1]

Received: 30 September 2023 / Accepted: 20 May 2024 / Published online: 2 July 2024

Abstract

As the main component of wearable electronic equipment, flexible pressure sensors have attracted wide attention due to their excellent sensitivity and their promise with respect to applications in health monitoring, electronic skin, and human–computer interactions. However, it remains a significant challenge to achieve epidermal sensing over a wide sensing range, with short response/recovery time and featuring seamless conformability to the skin simultaneously. This is critical since the capture of minute electrophysiological signals is important for health care applications. In this paper, we report the preparation of a nacre-like MXene/sodium carboxymethyl cellulose (CMC) nanocomposite film with a "brick-and-mortar" interior structure using a vacuum-induced self-assembly strategy. The synergistic behavior of the MXene "brick" and flexible CMC "mortar" contributes to attenuating interlamellar self-stacking and creates numerous variable conductive pathways on the sensing film. This resulted in a high sensitivity over a broad pressure range (i.e., 0.03–22.37 kPa: 162.13 kPa^{-1}; 22.37–135.71 kPa: 127.88 kPa^{-1}; 135.71–286.49 kPa: 100.58 kPa^{-1}). This sensor also has a low detection limit (0.85 Pa), short response/recovery time (8.58 ms/34.34 ms), and good stability (2000 cycles). Furthermore, we deployed pressure sensors to distinguish among tiny particles, various physiological signals of the human body, space arrays, robot motion monitoring, and other related applications to demonstrate their feasibility for a variety of health and motion monitoring use cases.

Gaofeng Wang and Lingxian Meng have contributed equally to this work.

✉ Shuiren Liu
lsrzzdx@zzu.edu.cn

[1] School of Materials Science and Engineering, Zhengzhou University, Zhengzhou 450001, China

[2] School of Materials Science and Engineering, National Institute for Advanced Materials, Nankai University, Tianjin 300350, China

Graphic abstract

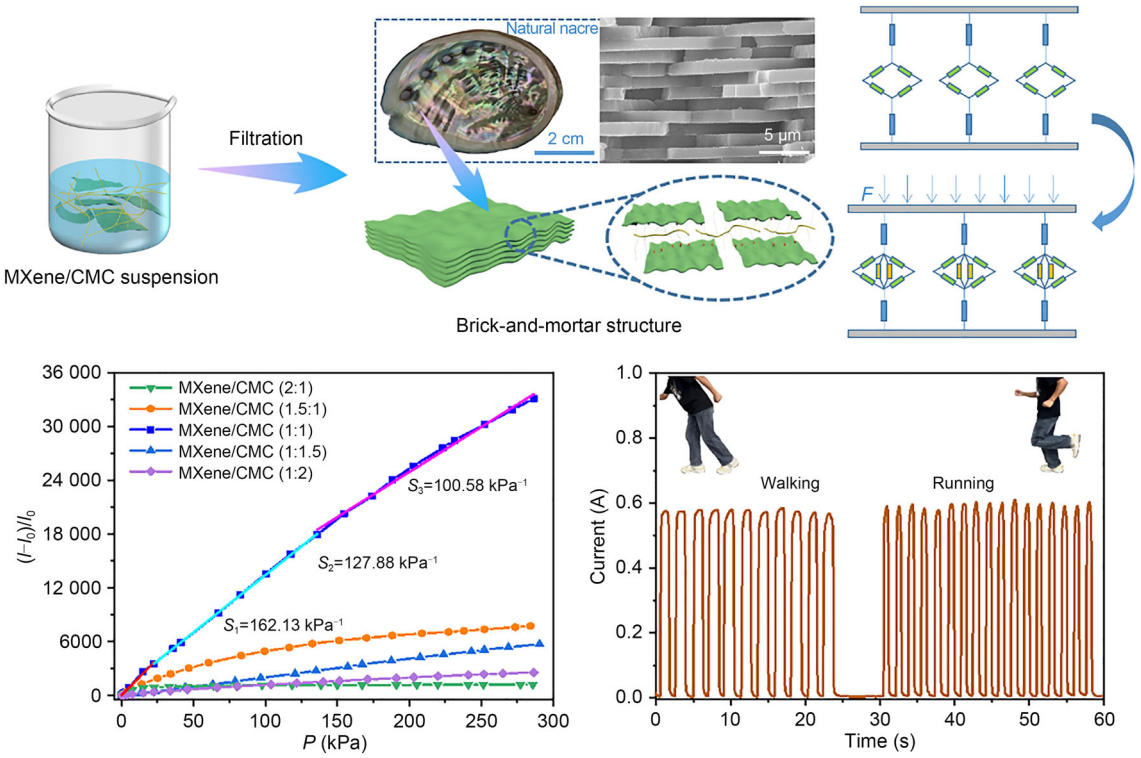

Keywords Flexible pressure sensor · MXene · Bioinspired · Physiological signals · Interlayer spacing

Introduction

Advancements in human–machine interaction (HMI) [1–3], electronic skin [4, 5], and the development of intelligent robots [6–9] have sparked an unprecedented demand for wearable sensors. Of all sensor types, flexible pressure sensors are highly sought after due to their exceptional sensing performance for mechanical stimuli and their ability to withstand stretching, bending, or twisting. These properties make them ideal for a variety of applications. In addition, via real-time monitoring of human activities [10–12] (e.g., limb movement, pronunciation, and facial expression) and physiological signal feedback [13–15] (e.g., pulse, jugular vein activity, electrocardiogram (ECG), and electromyography (EMG)), these sensors may be useful for health evaluations and/or disease diagnosis. Currently, piezoresistive pressure sensors, which use changes in electrical resistance caused by material deformation under applied pressure, are considered to be the most promising force-sensing technology. This is mainly due to the wide range of available active materials, their ease of fabrication, and the ease of integrating numerous processes during production.

In recent years, significant efforts have been made to enhance the detectability and sensitivity of piezoresistive sensors by optimizing the structural and electrical properties of the sensing materials used in their construction. These include: (i) incorporating microstructures on the electrode or dielectric layer [7, 16, 17], (ii) using composite dielectric materials [18, 19], and (iii) introducing engineered holes within the dielectric layer [20]. Notably, in this regard, engineering the microstructure of the electrode or sensing material is a common approach. Thus, sensors using microcolumns [21], micropyramids [22], microdomes [23], nanomesh [24], sponges [25], and aerogels [26] have all yielded impressive sensing performance results, achieving sensitivities beyond 100 kPa^{-1}. This enhanced performance can be attributed to the presence of nano/microstructures within the piezoresistive material. Under compression, these structures provide more conductive pathways than bulk structures, resulting in significant changes in the contact and/or internal resistance of sensing materials. Furthermore, the tailored low modulus (or low mass density) or hierarchical structure of sensing materials can contribute to high sensitivity and detection limits since the sensitivity of piezoresistive pressure sensors is generally inversely proportional to their

Young's modulus [14, 27]. However, most studies have shown lower sensitivity performance below 10 kPa [28, 29]. In addition, the material's inferior mechanical strength raises concerns regarding its ability to withstand long-term deformation and maintain structural integrity under high-pressure conditions [30–32].

In the natural world, nacre exhibits exceptional mechanical properties due in part to its specific brick-and-mortar layered structure. Researchers have successfully developed nacre-like nanocomposites that replicate its exceptional mechanical properties [33, 34]. In addition, nacre-like structures have been used to fabricate high-performance sensors. For example, Shi et al. [35] demonstrated that strain sensors based on a nanomimetic microscale "brick-and-mortar" architecture could offer a unique combination of ultrahigh sensitivity and large stretchability. Within this architecture, the $Ti_3C_2T_x$-Ag nanowire "brick" component imparts high electrical conductivity, while the poly(dopamine)/Ni^{2+} "mortar" component triggers synergistic toughening effects, including interfacial interactions, polymer chain stretching, and layer slippage. These mechanisms work together to absorb loading energy and effectively suppress crack propagation. In another study, Wang et al. [36] designed and prepared a bioinspired nacre-like intercalated MXene nanocomposite involving the assembly of a MXene/poly(3,4-ethylenedioxythiophene): poly(styrenesulfonate) (PEDOT:PSS)/polyvinyl alcohol (PVA) nanocomposite onto a flexible polyethylene (PE) film substrate. The assembled flexible wearable epidermic sensor exhibited short response/recovery time, a broad working range, and excellent sensing performance. Moreover, the high conformability of the layered architecture on top of the human skin enabled it to detect subtle electrophysiological signals (i.e., ECG and EMG signals) that can be used to evaluate health status. However, the incorporation of stimulative substances to achieve multistimuli-responsive actuation has led to limitations in sensitivity. Thus, despite their potential usefulness for motion detection or health care applications, the realization of high-performance sensors capable of high sensitivity, a broad sensing range, short response/recovery time, and seamless conformability to the skin still presents a formidable challenge.

In this work, we present a bioinspired approach to achieve co-optimized sensitivity and operating range of a pressure sensor based on the "brick-and-mortar" architecture. The nacre-mimetic pressure sensor described here uses hydrophilic two-dimensional (2D) titanium carbide ($Ti_3C_2T_x$) MXene nanosheets as the "brick" and flexible one-dimensional (1D) carboxymethyl cellulose (CMC) fibers as the "mortar." Moreover, it is constructed using a scalable "vacuum-assisted filtration" method. CMC was selected due to its greater cost-effectiveness, degradability, and biocompatibility compared to polymeric materials such as PVA, dopaminehydrochloride (DAH), and polypyrrole (PPy) [37]. The intercalation of the flexible CMC "mortar" effectively alleviates the layer stacking of MXene nanosheets and expands their interlayer spacing. In addition, sufficient conductive pathways between the MXene nanosheets are preserved for substantial changes to occur in the contact and/or internal resistance of the structured sensing materials when under pressure. Furthermore, the incorporation of CMC enhances the mechanical performance of the nano composites, rendering them more stable for sensing applications. The resulting nacre-like MXene/CMC-based pressure sensors were found to show excellent sensitivity (i.e., up to 162.13 kPa^{-1}) in the range of 0.03–22.37 kPa, a maximum working range of 286.49 kPa (sensitivity of 100.58 kPa^{-1}), a minimum detection limit of 0.85 Pa, short response/recovery time (8.58 ms/34.34 ms), and stable fatigue resistance (2000 cycles). Thus, based on their excellent sensing performance, they may be employed for monitoring full-range pressure detection, from tiny subtle human pulse and neck vein movements to human activities such as finger movements, vocal cord vibration, walking, and running. Moreover, the high conformability of the layered architecture with human skin enables it to detect subtle electrophysiological signals (i.e., ECG and EMG signals) for the evaluation of human health status.

Experimental section

Materials

The Ti_3AlC_2 powder (MAX, 99.8%, 400 mesh) was purchased from Laizhou Kai Kai Ceramic Materials Co., Ltd. (China). Hydrochloric acid (HCl, 12 mol/L) and LiF were purchased from Luoyang Haohua Chemical Reagent Co., Ltd. (China) and Shanghai Aladdin Biochemical Technology Co., Ltd. (China), respectively. CMC (viscosity 800–1200 mPa·s) was purchased from Shanghai Klamar Reagent Co., Ltd. (China). Filter paper, light-emitting diodes (LEDs), and robots were purchased from Taobao. Milli-Q water (18.25 MΩ) was used to prepare all solutions.

Preparation of MXene nanosheets

LiF (2 g) and HCl (40 mL, 9 mol/L) were mixed and stirred for 30 min to disperse, after which 2 g MAX powder was slowly added. After magnetic mixing and etching at 35 °C for 24 h, ultrasonication was performed for 5 min. Next, centrifugation was repeated at 3500 r/min for 10 min until the liquid reached a pH of 5. The precipitate was then intercalated with ethanol, followed by ultrasonication for 20 min and centrifugation at 10,000 r/min for 20 min. The resulting precipitation was then ultrasonicated with added water for 20 min. Finally, the

mixture was centrifuged at 3500 r/min for 5 min, and the upper solution, MXene, was collected for later use.

Fabrication of the MXene/CMC pressure sensor

To identify the best preparation, we prepared MXene and CMC solutions with different mass ratios (i.e., 2:1, 1.5:1, 1:1, 1:1.5, and 1:2). Each of these solutions was mixed and subjected to an ultrasonic treatment for 20 min before being stirred for 2 h to obtain a uniformly mixed solution. Subsequently, a MXene/CMC composite membrane was obtained via simple vacuum filtration, and this was then cut into appropriately-sized pieces for performance testing. Subsequently, the above samples were placed on polyethylene terephthalate (PET) and polyimide (PI) substrates with silver as interdigitated electrodes, and two copper wires were connected to both ends of the electrodes using silver paste. Finally, a pressure sensor for further measurement was obtained by packaging with a PE film. MXene/PVA and MXene/DAH sensors were prepared by using a process similar to the MXene/PVA (MXene/DAH) at a mass ratio of 1:1.

Characterization and measurements

The morphology and size of MXene nanosheets were characterized by the atomic force microscope (AFM) (JPK BIOAFM, Germany). The surface, cross-sectional morphology, and elemental composition of the MXene/CMC films were characterized via scanning electron microscope (SEM) (ZEISS GeminiSEM 300, Carl Zeiss, Germany). X-ray diffraction (XRD) (SmartLab SE, Rigaku, Japan) and X-ray photoelectron spectroscopy (XPS) (K-Alpha, Thermo Fisher Scientific, USA) were used to further characterize the chemical compositions and structure of the films. Fourier transform infrared spectroscopy (FTIR) spectrum data were tested using a Thermo Scientific Nicolet IS20 instrument. The sensing performance of the MXene/CMC film pressure sensor was then tested on a system consisting of a computer-controlled Shimadzu AGS-X and a source meter Keithley 2450. The constant voltage input used during the test was 1 V.

Signal measurement of physiological and human activities

The assembled sensor was attached to a human volunteer to measure various movements and physiological signals produced by the human body. These included finger movements, wrist movements, blowing, swallowing, and speaking, as well as pulse, internal jugular vein (IJV), ECG, and EMG measurements. For ECG and EMG signal testing, medical tape was used to attach the electrodes to the inner arm of the human body. The corresponding electrophysiological signals were measured using an electrochemical workstation (CHI 660E). Other test data were collected using a digital source meter.

Fabrication of a sensor array based on the MXene/CMC pressure sensor

We prepared 4×4 interdigitated electrodes (15 mm×8 mm) by evaporating silver particles. The sensor array was obtained after assembling 16 suitably-sized MXene/CMC composite films onto the 4×4 interdigitated electrode using a PE film.

Fabrication of a wireless display based on the MXene/CMC pressure sensor

The sensor was then installed on the leg joint of a remotely controlled robot, and copper wire was used to connect it to the digital source meter and UNI-T UT61E+. Real-time robot movement signals were then wirelessly transmitted to a mobile phone using a UNI-T UT61E+ Bluetooth module.

Results and discussion

Material synthesis and characterization

MXene/CMC sensing layer using the "brick-and-mortar" structure was prepared using a vacuum-assisted extraction method (Figs. 1a and 1b). First, a MXene colloidal suspension was obtained by selectively etching the Al atomic layer on the Ti_3AlC_2 MAX phase using a wet chemical-etching strategy [38, 39]. Moreover, the CMC solution was obtained via ultrasonic oscillation. Thereafter, the above aqueous suspensions were uniformly mixed for vacuum-assisted lamella self-assembly to obtain a free-standing film (Fig. 1c). Due to the driving force of vacuum filtration and hydrogen bonding between MXene and CMC, the desired brick-and-mortar structure was achieved. In addition, the pressure sensor was fabricated by assembling the MXene/CMC film and the Ag fork-finger electrode PET membrane in a face-to-face orientation. This was then encapsulated using PE in view of the stability of the membrane (Fig. 1d). Furthermore, the layered architecture's high conformability with the skin gives it the potential to detect and monitor subtle electrophysiological signals such as ECGs and EMGs, thereby permitting human health status assessment (Fig. 1e).

To validate the successful preparation of the MXene/CMC films, a series of physicochemical characterizations were performed following the preparation process. An AFM showed that the thickness of the MXene nanosheet was approximately 1.88 nm and its horizontal span was approximately 2.483 μm (Fig. 2a). These findings were consistent with the likely single-layer structure of the MXene nanosheet [40].

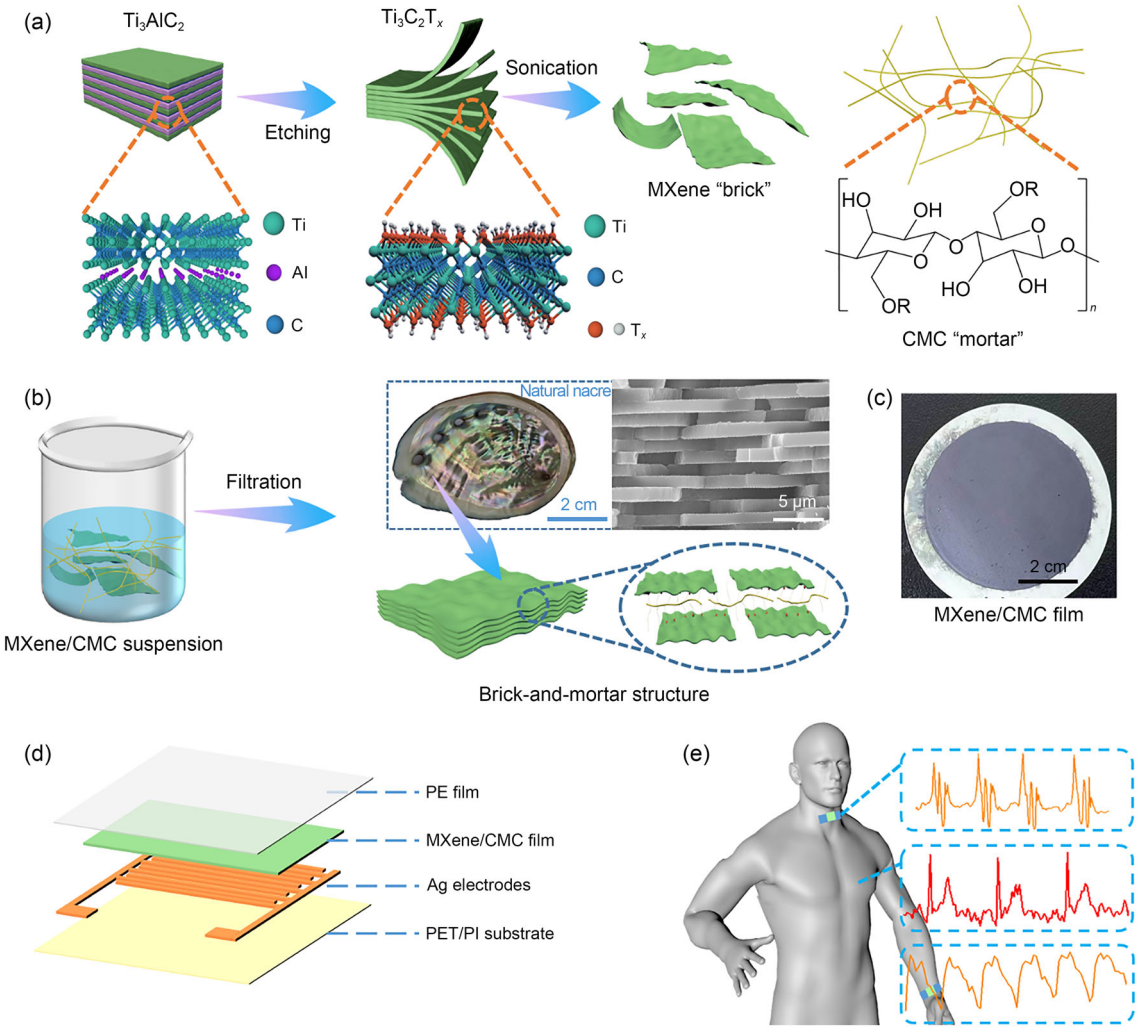

Fig. 1 **a**, **b** Schematic fabrication of MXene/carboxymethyl cellulose (CMC) with a "brick-and-mortar" structure. **c** Optical photo of the MXene/CMC composite film. **d**, **e** Schematic illustration of the MXene/CMC film-based flexible pressure sensor and its application for human healthcare. PE: polyethylene; PET: polyethylene terephthalate; PI: polyimide

Next, XRD spectrum data (Fig. 2b) revealed a (002) peak at 6.32°, indicating the increased layer spacing of MXene after etching. In addition, XPS was performed to analyze the composition of the MXene and MXene/CMC films (Fig. 2c). Here, peaks of Ti 2p, C 1s, O 1s, and F 1s appeared at 455.4, 284.8, 532.6, and 685.3 eV, respectively (Fig. S1 in Supplementary Information). These data further verified the successful preparation of MXene [41, 42]. Furthermore, Na 1s XPS data for the MXene/CMC composite membrane indicated the effective recombination of MXene and CMC (Fig. S2 in Supplementary Information).

Considering that CMC content has a significant impact on the properties of MXene/CMC composite membranes, we prepared samples with varied mass ratios (i.e., 2:1, 1.5:1, 1:1, 1:1.5, and 1:2) to assess the magnitude of its influence (Fig. S3 in Supplementary Information). As depicted by the XRD spectral characterization (Fig. 2d), the (002) peak shifts downward with increasing CMC content, demonstrating that the augmentation in CMC content will amplify the layer spacing of MXene. Moreover, as illustrated by FTIR (Fig. 2e), the CMC exhibits a strong absorption band at 2918 cm^{-1}. This can be attributed to the expansion vibration of C–H. Moreover, characteristic peaks at 1584, 1416, and 1328 cm^{-1} are correlating to the expansion vibration of COO–. Finally, characteristic peaks of MXene at 2930 and 3440 cm^{-1} can be attributed to the stretching vibration of –CH and –OH groups. The –OH group shifted to 3470 cm^{-1} in MXene/CMC films, which suggested a hydrogen bonding interaction between CMC and MXene [37, 43]. In addition, the above characteristic peaks are present in MXene/CMC films, demonstrating that there are interactions between these two components. For example, scanning electron microscope (SEM) images

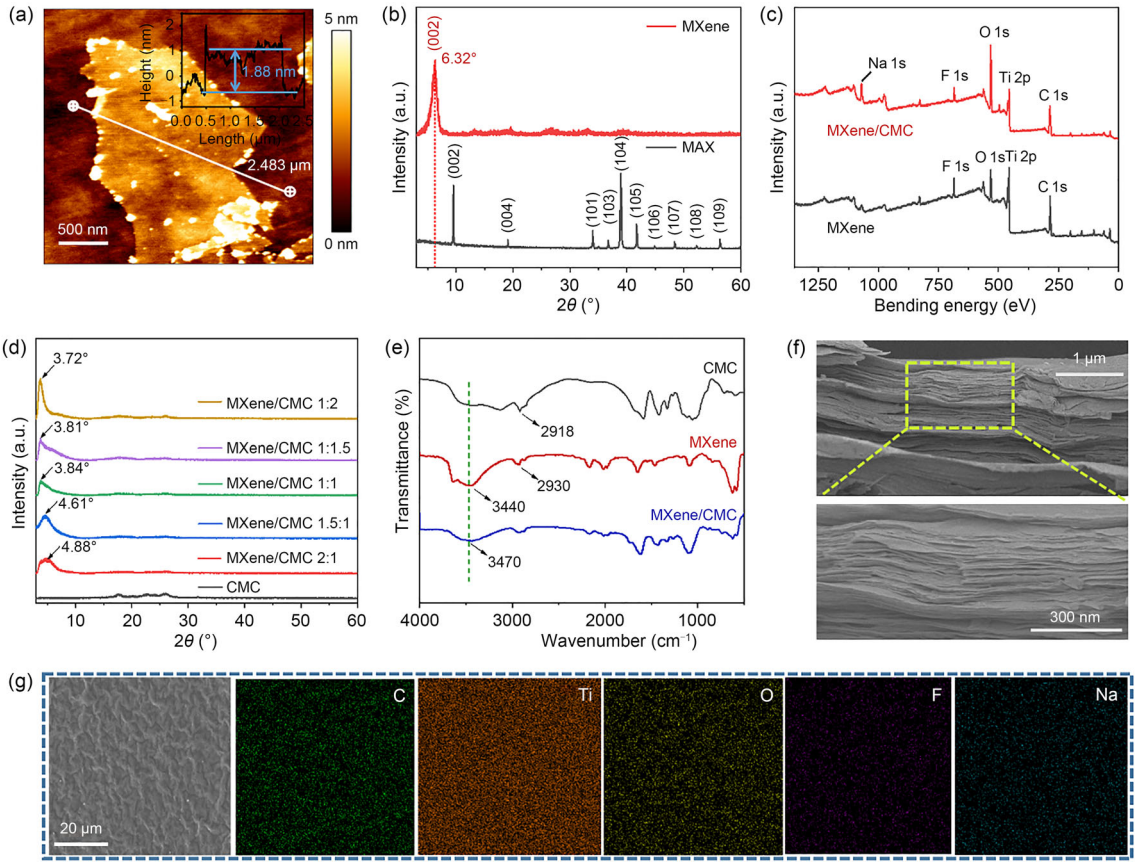

Fig. 2 **a** Atomic force microscope (AFM) image of the MXene nanosheet. **b** X-ray diffraction (XRD) spectra of MAX and MXene. **c** X-ray photoelectron spectroscopy (XPS) survey spectra of MXene and MXene/carboxymethyl cellulose (CMC) films. **d** XRD patterns of MXene films with different CMC mass ratios. **e** Fourier transform infrared spectroscopy (FTIR) data for MXene, MXene/CMC, and CMC. **f** Cross-sectional scanning electron microscope (SEM) images of the MXene/CMC film. **g** Surface SEM image of the MXene/CMC film and corresponding elemental mapping images of the MXene/CMC film for C, Ti, O, F, and Na

of the cross-section of the MXene/CMC composite membrane (Fig. 2f and Fig. S4 in Supplementary Information) revealed the parallel-arranged, neat, and compact layered structure of MXene. Moreover, CMC was evenly distributed between MXene layers as an adhesive, thereby successfully constructing the desired "brick-and-mortar" interface structure. However, no curly CMC fiber elastic fibers such as those in the CMC powder (Fig. S5 in Supplementary Information) were observed in the cross-sectional SEM image shown in Fig. S6 (Supplementary Information). This phenomenon is due to the high dispersibility and small size of monodisperse CMC in water (Fig. S5 in Supplementary Information). In addition, Fig. 2g shows that the surface of the MXene/CMC composite membrane has corrugated folds. Furthermore, the uniform distribution of C, Ti, O, F, and Na elements observed in Fig. 2g and Fig. S6 (Supplementary Information) reveals the energy dispersion spectrum, further confirming the uniform distribution of CMC. This "brick-and-mortar" structure significantly improves the mechanical strength and flexibility of the hybrid film. As a result, the MXene/CMC film obtained here demonstrates superior tensile strength (i.e., 49.55 MPa) compared to either the MXene or CMC films (Fig. S7 in Supplementary Information), which showed respective breaking strengths of 36.98 and 33.77 MPa, respectively. This shows its exceptional flexibility. Subsequently, to explore the influence of CMC on the electrical properties of MXene, we characterized the square resistance of the MXene/CMC films using different proportions of the two components. Figure S8 (Supplementary Information) shows that the sheet resistance increases with increasing CMC content, which are 0.845, 14.250, 139.200, 738.000, and 1535.000 Ω/□ respectively. Thus, adding CMC causes a reduction in the electrical conductivity of the MXene/CMC composite films.

Working mechanism and sensing properties of the MXene/CMC pressure sensor

We employed an electrical signal test system that included a source meter, force gauge, single-axis motion controller, and computer to evaluate the pressure-sensing performance of the device. To verify the influence of CMC content on sensing performance, we prepared MXene/CMC pressure sensors with different mass ratios (i.e., 2:1, 1.5:1, 1:1, 1:1.5, and 1:2) by controlling a single variable. Under the dynamic and static conditions of electrical signal testing, a series of experiments were conducted to determine the electrical properties of the MXene/CMC piezoresistive sensor. The test system was driven by a voltage of 1 V to measure changes in the output signal response of the external pressure in real time.

As shown in Fig. 3a and Figs. S9 and S10 (Supplementary Information), the MXene/CMC pressure sensor with a mass ratio of 1:1 exhibited the best pressure sensitivity. The sensitivity values for the low-pressure range (0.03–22.37 kPa), the medium-pressure range (22.37–135.71 kPa), and the high-pressure range (135.71–286.49 kPa) were 162.13 kPa^{-1}(S_1), 127.88 kPa^{-1}(S_2), and 100.58 kPa^{-1}(S_3), respectively. Compared to the sensors assembled using pure MXene or other nanocomposite films such as MXene/PVA and MXene/DAH, the MXene/CMC pressure sensor showed the best sensing performance. Figure 3b shows the monitoring of the current–time (I–T) curves under continuously applied pressure. We observed monotonically increases in response to increasing pressure, mainly due to the increasing contact area and conductive path between MXene nanosheets. The significantly increased on/off ratio of the current with pressure application further confirms the device's ability to rapidly distinguish between varying levels of pressure. In addition, by applying a scanning voltage of −1 to 1 V to the device, as depicted in Fig. 3c, all current–voltage (I–V) curves under different external pressures exhibited a good linear relationship, indicating good Ohmic contact between the sensing layer and the interdigital electrode. Although elastic deformation of the substrate can lead to a certain response time lag/delay, the device shows short response/recovery time of 8.58 ms/34.34 ms under a pressure of 2.26 kPa (Fig. 3d). This is equivalent to the response time of the human body and skin, and is convenient for monitoring the movement of the human body. In addition, Fig. 3e shows that the pressure sensor can identify external pressures (i.e., 1.22 and 10.22 kPa) at different speeds and frequencies with a stable and lasting response. Furthermore, the curves shown for I–T and pressure–time (P–T) (Fig. 3f) were consistent under the periodic pressure test at a fixed pressure (3.2 kPa); this demonstrates the short response time and superior performance of the piezoresistive sensor reported here. Next, the real-time measured values of relative current changes under cyclic loadings/unloadings with different pressures were also observed (Fig. 3g), and the measured current changed repeatedly in response to applied pressure, which further demonstrates the robustness and reliability of the sensor. Finally, to further evaluate the stability and durability of the pressure sensor, a pressure cycling test was carried out. After 2000 pressure cycling tests under a pressure of 124.1 kPa, the sensor still maintained relative stability, as shown in Fig. 3h. In addition, the pressure sensor still showed good cycling stability at low pressures (Fig. S11 in Supplementary Information). Figure 3i shows the sensitivity of the sensor relative to the reported results. The developed sensor not only showed high sensitivity but also an incomparably broad pressure-sensing range, i.e., up to 286.49 kPa. Its performance is therefore superior to that of many existing excellent pressure sensors [34, 36, 40, 44–53].

The construction of a high-performance pressure sensor relies on substantial changes in the contact and/or internal resistance of the structured sensing materials under pressure. In this study, MXene nanosheets are endowed with a layered parallel structure, which allows them to provide more conductive paths under pressure. Moreover, the MXene nanosheets are easily stacked due to the van der Waals force; thus, the initial conductivity of the MXene films is high, which is not conducive to high sensitivity. In addition, the layered structure formed between the MXene nanosheets easily collapses and cannot recover to the initial state, making it difficult to possess high sensitivity and stable sensing performance. However, owing to the intercalation of the CMC, the MXene nanosheets can be effectively separated to form a relatively stable lamellar structure. Conversely, sufficient conductive points between MXene nanosheets are preserved [54, 55], which ensures that there are sufficient variable conductive contact points between the nanosheets.

A schematic of the working mechanism of the pressure sensor is illustrated in Fig. 4a. The resistance between the sensing layer and the interdigital electrode is simplified as a circuit model, as shown in Fig. 4b. In the static state, the load of the sensing device mainly includes the electrode resistance R_e, the contact resistance R_c, and the fixed resistance R_{MX}. Under pressure, the interlayer spacing decreases, and the internal resistance R_{CMC} is connected in parallel to R_{MX}. This is then connected in series with R_e and R_c, such that the total resistance of the sensor device is reduced. In addition, by varying the CMC content between MXene nanosheets, the optimal structural properties can be obtained. When a small amount of CMC is added, the plane-to-plane contact area between the MXene layers remains relatively large, and the degree of deformation can easily reach saturation under pressure. However, as the CMC content increases, the interlayer spacing of MXene creates additional conductive pathways between the MXene nanosheets. When subjected to pressure, the material then undergoes complete compression, decreasing interlayer spacing and causing an increase in the contact area between adjacent layers. The synergistic

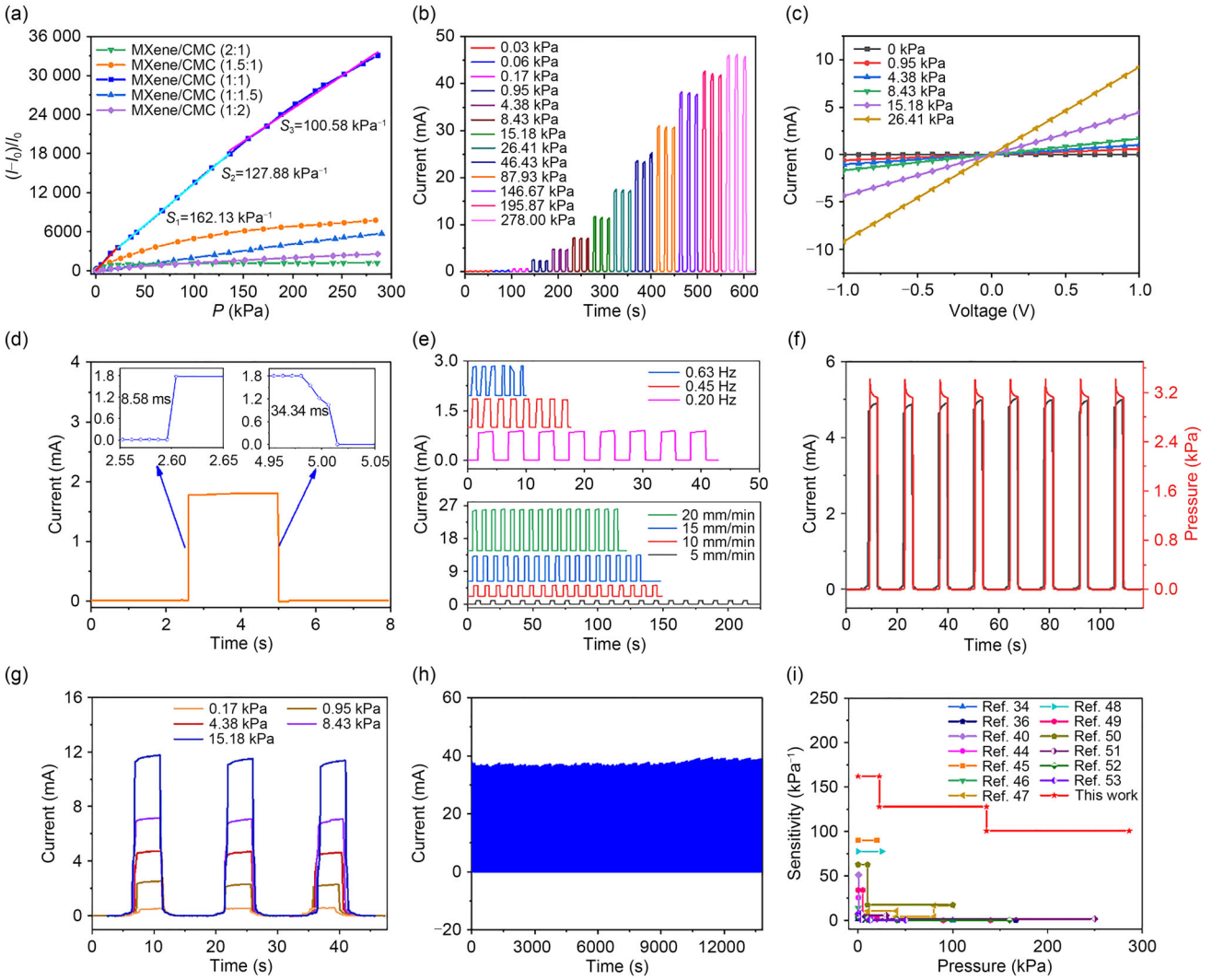

Fig. 3 Sensing performance of the MXene/carboxymethyl cellulose (CMC) pressure sensor. **a** Sensitivity comparison of MXene/CMC pressure sensors with different mass ratios. **b** *I*–*T* curves. **c** *I*–*V* curves. **d** Response/recovery time. **e** Response at different loading speeds under 1.22 kPa (bottom) and response at different loading frequencies under 10.22 kPa (top). **f** Interactions between $I-T$ and $P-T$ curves. **g** Responses at different pressure levels under three cyclic loadings/unloadings. **h** 2000 pressure cycling tests of the MXene/CMC pressure sensor at 124.1 kPa. **i** Sensitivity comparison of our pressure sensor with existing piezoresistive sensors [34, 36, 40, 44–53]

effect of decreasing plane-to-plane contact and increasing the number of variable conductive contact points enhances the alterable conductive paths between the MXene nanosheets, and results in a significant decrease in resistance and an increase in current under pressure. After the pressure is removed, the sensing layer gradually returns to the initial state due to the flexibility and elasticity of the material itself. However, when the CMC content becomes too high, most of the CMC remains embedded between the MXene nanosheets, decreasing the number of conductive contact points between the MXene nanosheets sharply. This leads to a decrease in the relative contact area of the sensing layer and causes low sensor sensitivity. Finally, as shown in Fig. S9 (Supplementary Information), the best sensitivity and sensing performance of the sensing layer are achieved when the content ratio of MXene to CMC is 1:1.

Practical applications of the MXene/CMC pressure sensor

For flexible pressure sensors, a high detection limit and a large working range are key factors in determining the range of potential sensor applications. Given that this sensor shows excellent sensing performance, including high sensitivity, a wide working range, short response/recovery time, good flexibility, and good stability, we speculated that the MXene/CMC pressure sensor can be applied for full-range pressure monitoring. As shown in Fig. 5a, the sensor can be

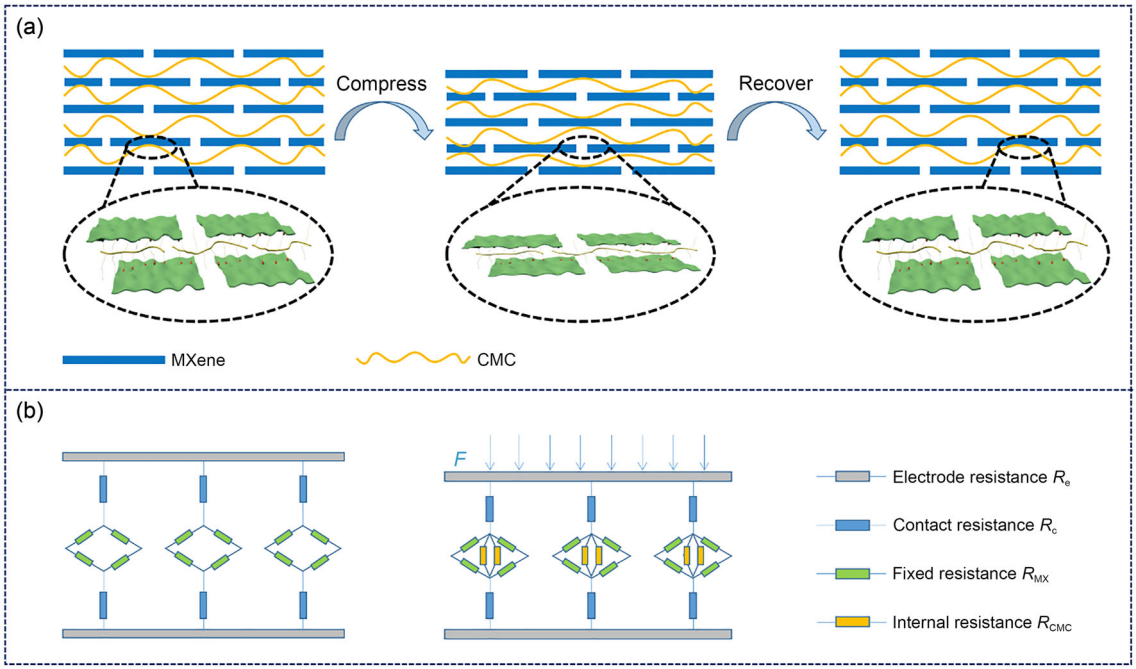

Fig. 4 Sensing mechanism. **a** Schematic of the working mechanism of the MXene/carboxymethyl cellulose (CMC) pressure sensor. **b** Sensing model and equivalent circuit resistance

adhered to the sole of a shoe to identify changes in pressure signals during human movement. Subsequently, we attached the sensor to different muscles and joints of the human body, and different current waveform signals were observed. As shown in Fig. 5b, when the sensor is attached to the fingers of the volunteers, it may be beneficial to detect early osteoarthritis and could be useful in finger-related rehabilitation training by detecting different finger bending angles. In addition, the bending signal of a larger joint, such as the wrist, can be determined (Fig. S12a in Supplementary Information). When the sensor is placed on the facial muscles and throat, expression signals corresponding to smiling and swallowing actions can be clearly recognized (Figs. S12b and S12c in Supplementary Information). The high sensitivity of this sensor also enables it to detect subtle changes in pressure signals. As shown in Fig. S12d (Supplementary Information), the MXene/CMC-based sensor can detect the loading and removal of tiny particles, as exemplified by the detection of small differences in the loading amounts of rice particles (0.85 Pa), mung bean (1.98 Pa), and soybean (4.36 Pa); this further demonstrates its high detection accuracy. Furthermore, due to its relatively low detection limit, the difference between slow exhalation and rapid blowing can be detected as a rapid but significant change in the current signal (Fig. 5c). The sensor can also accurately distinguish the current intensity and time interval of finger pressing (Figs. S12e and S12f in Supplementary Information). Therefore, this sensor could be used to monitor tremors, including those related to Parkinson's disease, which have a characteristic frequency of 4–6 Hz. The sensitivity of this sensor could therefore facilitate real-time early diagnosis of Parkinson's disease (Fig. S12g in Supplementary Information). In another potential application, the sensor could also be used for sound detection. As shown in Fig. 5d, when a tester utters a word, he can receive a periodic response signal of the corresponding word current according to the different vibrations involved in pronouncing that specific word.

To accurately obtain information related to human health status in clinical tests, various instruments are used, and many of these are both expensive and limited by the production of a single signal. Signals such as the pulse wave are important physiological signs for evaluating blood pressure, heart rate, and arteriosclerosis status, among others. Accordingly, to study the pulse beat change, we placed a sensor close to the wrist of a volunteer. As shown in Fig. 5e, the pulse wave and its corresponding characteristic peaks, including percussion, tidal, and dicrotic waves, were simple to visualize. These tests measured the pulse rate of the subject at about 70 times/min. Furthermore, this sensor can be attached to the neck, where it could directly measure and monitor the central blood pressure waveform and pulsation of the IJV in a noninvasive way (Fig. 5f). In addition, ECG is one of the most important electrophysiological signals used in the diagnosis of heart-related diseases. Therefore, we assembled MXene/CMC composite membranes into skin sensing electrodes and attached them to volunteers' arms. As shown in Fig. 5g, ECG signals (79 beats/min) with P_E wave, Q_E, R_E, and S_E complex, and T_E wave characteristics were identified. This indicated that the

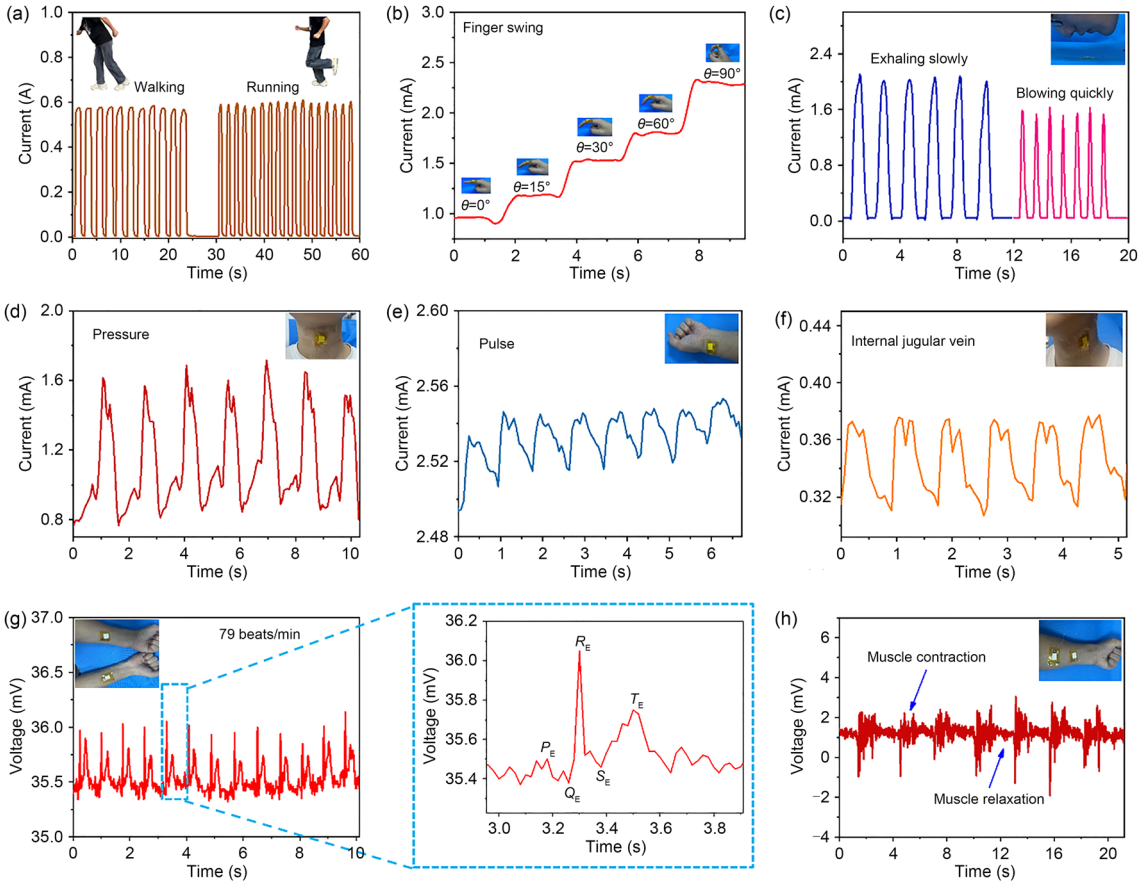

Fig. 5 Application (group I) demonstration of the MXene/carboxymethyl cellulose (CMC) pressure sensor. **a** Current response of the signal when walking or running. **b** Current response of the sensor during finger bending movements of different angles. **c** Current response during slow exhalation or rapid blowing. **d** Current response for speaking the word "pressure." **e** Current response of the pulse at the wrist. **f** Current response of the internal jugular vein (IJV) pulse. **g** Voltage response of electrocardiogram (ECG) signals. **h** Voltage response of electromyography (EMG) signals

heart rates of the focal volunteers were normal (i.e., 60–100 beats/min in healthy people). Moreover, EMG signals could be detected by having volunteers repeatedly clench their fists (Fig. 5h). All of these test results were consistent with those of normal, healthy volunteers, and therefore these tests prove the feasibility of using this sensor for medical health monitoring. To further explore novel application potentials of these pressure sensors, a series of application scenarios involving intelligent electronic products that incorporated the sensor were designed. First, in view of the excellent high conductivity of the MXene/CMC pressure sensor, we connected it to an LED light board to construct a series circuit. During the test, a voltage of about 3 V was supplied to the circuit. As shown in Fig. 6a, three distinct mass weights were placed, and as the weight increased, the luminosity of the LED lamp correspondingly intensified. In addition, the pressure on the sensor was further fine-tuned by changing the strength of the finger press applied. It was discovered that as the pressure increased, the current subsequently amplified, and the LED lights grew brighter (Video S1 in Supplementary Information). Therefore, we speculate that the sensor could be used as a rheostat for pressure regulation to protect the circuit from excessive current. In addition, a 4×4 pressure sensor array was built to explore its ability to sense pressure distribution. After placing two weights of differing mass on the array, we observed that the LED lights exhibited varying luminosity on the corresponding units situated on the portions of the array in contact with the weights (Fig. 6b). Furthermore, by pressing different positions of the array, the brightness and position of the corresponding LED lamps can change accordingly (Video S2 in Supplementary Information). Taken together, these results indicate that the general shape and pressure distribution of a specific object can be analyzed by referring to the current intensity of each matrix point qualitatively and quantitatively. Finally, we explored a potential application involving precise robot control and intelligent prosthesis. To do so, a sensor was installed on the leg joints of a robot. Here the sensor could clearly detect the real-time motion state of

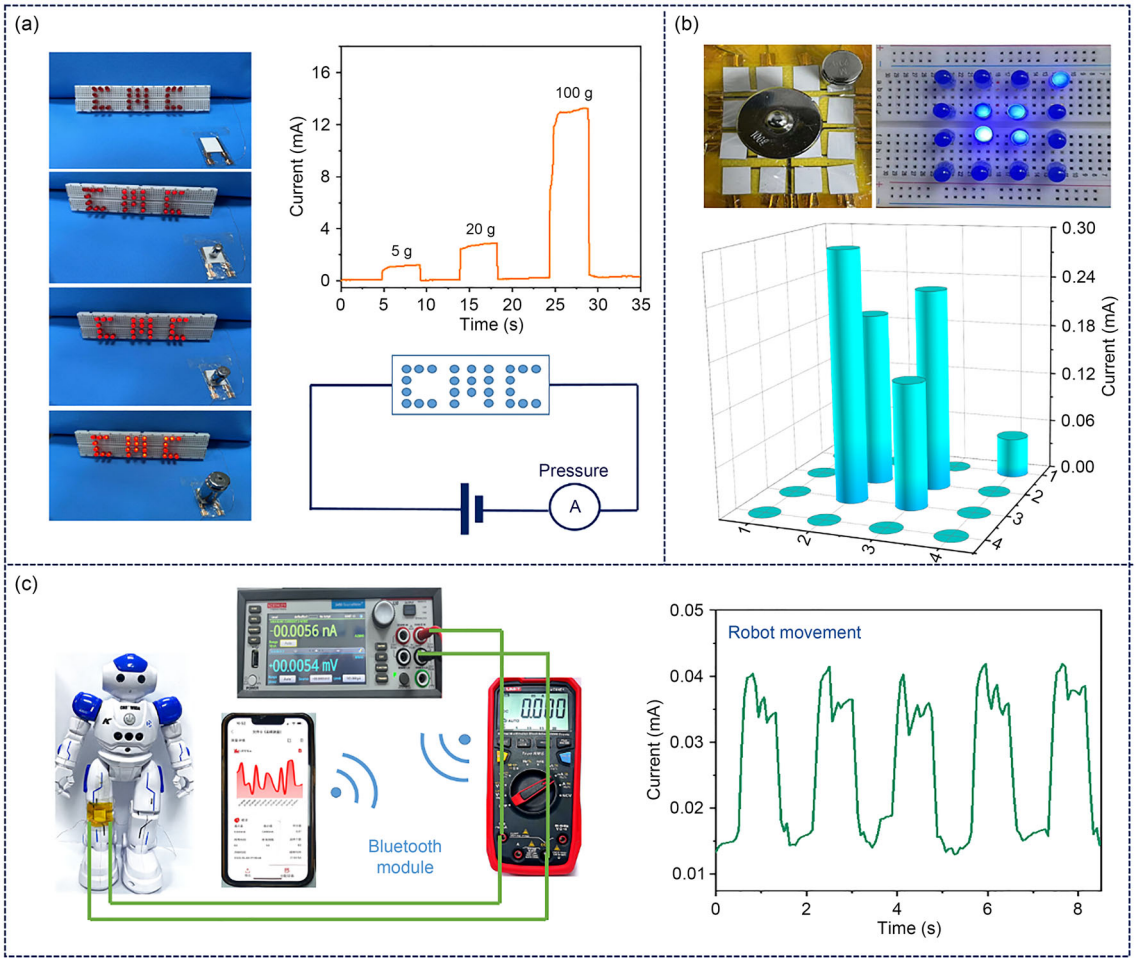

Fig. 6 Application (group II) demonstration of the MXene/carboxymethyl cellulose (CMC) pressure sensor. **a** Current response of the pressure signals controlling the brightness of an light-emitting diode (LED) via the sensor. **b** Photos of a 4×4 pressure-sensing array and detection of pressure distribution. **c** Photograph of the pressure sensor assembled on a robot and its response to movement behaviors as measured using a Bluetooth circuit module

the robot using a wireless display and a Bluetooth module (Fig. 6c and Video S3 in Supplementary Information). In conclusion, these results indicate that the sensor described in this paper has numerous promising applications in the fields of personal health monitoring and wearable electronic devices.

Conclusions

In this work, a type of nacre-like layered "brick-and-mortar" interface structure was constructed using a simple vacuum filtration method. Moreover, we explored its application as a high-performance, multifunctional piezoresistive pressure sensor. The pressure sensor exhibited high sensitivity (i.e., 0.03–22.37 kPa: 162.13 kPa^{-1}), a wide linear range (0.03–286.49 kPa), short response/recovery time (8.58 ms/34.34 ms), a low detection limit (0.85 Pa), and high stability (2000 cycles). More importantly, the practical applications of the sensor for detecting and identifying tiny particles and the feasibility of using it as a protective layer for electronic skin and commercial LED circuits were also investigated, thereby demonstrating promising potential applications in the fields of space array identification, wireless Bluetooth portable detection devices, and wearable electronic equipment.

Supplementary Information The online version contains supplementary material available at https://doi.org/10.1007/s42242-024-00292-4.

Acknowledgements This work was supported by the National Natural Science Foundation of China (Nos. 52003253 and 52203245), the China Postdoctoral Innovative Talent Support Program (No. BX20220274), and the Henan Science and Technology Department, China (No. 222301420004).

Author contributions SRL and XYL guided the whole project. GFW and SRL conceived the idea, and designed the experiments and methodology. GFW and LXM analyzed the data and drafted the manuscript. XYJ and JJL participated in the discussion for experiments. All the authors approved the submission.

Declarations

Conflict of interest All the authors declare that they have no conflict of interest.

Ethical approval All volunteers signed the informed written consent prior to the research for the human activity experiments.

References

1. Zhong MJ, Zhang LJ, Liu X et al (2021) Wide linear range and highly sensitive flexible pressure sensor based on multistage sensing process for health monitoring and human-machine interfaces. Chem Eng J 412(15):128649. https://doi.org/10.1016/j.cej.2021.128649
2. Shi ZY, Meng LX, Shi XL et al (2022) Morphological engineering of sensing materials for flexible pressure sensors and artificial intelligence applications. Nano-Micro Lett 14(1):141. https://doi.org/10.1007/s40820-022-00874-w
3. Li MK, Zhang YF, Lian LSY et al (2022) Flexible accelerated-wound-healing antibacterial MXene-based epidermic sensor for intelligent wearable human-machine interaction. Adv Funct Mater 32(47):2208141. https://doi.org/10.1002/adfm.202208141
4. Niu H, Li H, Gao S et al (2022) Perception-to-cognition tactile sensing based on artificial-intelligence-motivated human full-skin bionic electronic skin. Adv Mater 34(31):2202622. https://doi.org/10.1002/adma.202202622
5. Fu XY, Wang LL, Zhao LJ et al (2021) Controlled assembly of MXene nanosheets as an electrode and active layer for high-performance electronic skin. Adv Funct Mater 31(17):2010533. https://doi.org/10.1002/adfm.202010533
6. Ma YN, Cheng YF, Wang J et al (2022) Flexible and highly-sensitive pressure sensor based on controllably oxidized MXene. InfoMat 4(9):e12328. https://doi.org/10.1002/inf2.12328
7. Cheng YF, Ma YN, Li LY et al (2020) Bioinspired microspines for a high-performance spray $Ti_3C_2T_x$ MXene-based piezoresistive sensor. ACS Nano 14(2):2145–2155. https://doi.org/10.1021/acsnano.9b08952
8. Li L, Cheng YF, Cao HH et al (2022) MXene/rGO/PS spheres multiple physical networks as high-performance pressure sensor. Nano Energy 95:106986. https://doi.org/10.1016/j.nanoen.2022.106986
9. Zhang JZ, Sun DD, Zhang B et al (2022) Intrinsic carbon nanotube liquid crystalline elastomer photoactuators for high-definition biomechanics. Mater Horiz 9(3):1045–1056. https://doi.org/10.1039/d1mh01810h
10. Hou YX, Wang L, Sun R et al (2022) Crack-across-pore enabled high-performance flexible pressure sensors for deep neural network enhanced sensing and human action recognition. ACS Nano 16(5):8358–8369. https://doi.org/10.1021/acsnano.2c02609
11. Yang M, Cheng YF, Yue Y et al (2022) High-performance flexible pressure sensor with a self-healing function for tactile feedback. Adv Sci 9(20):e2200507. https://doi.org/10.1002/advs.202200507
12. Guan M, Liu Y, Du H et al (2023) Durable, breathable, sweat-resistant, and degradable flexible sensors for human motion detection. Chem Eng J 462:142151. https://doi.org/10.1016/j.cej.2023.142151
13. Meng KY, Xiao X, Wei WX et al (2022) Wearable pressure sensors for pulse wave monitoring. Adv Mater 34(21):e2109357. https://doi.org/10.1002/adma.202109357
14. Shi XL, Fan XQ, Zhu YB et al (2022) Pushing detectability and sensitivity for subtle force to new limits with shrinkable nanochannel structured aerogel. Nat Commun 13(1):1119. https://doi.org/10.1038/s41467-022-28760-4
15. Song YY, Ren WJ, Zhang YQ et al (2023) Synergetic monitoring of both physiological pressure and epidermal biopotential based on a simplified on-skin-printed sensor modality. Small 19(45):e2303301. https://doi.org/10.1002/smll.202303301
16. Du WW, Li ZK, Zhao YL et al (2022) Biocompatible and breathable all-fiber-based piezoresistive sensor with high sensitivity for human physiological movements monitoring. Chem Eng J 446:137268. https://doi.org/10.1016/j.cej.2022.137268
17. Wu ZY, Liu SR, Hao ZJ et al (2023) MXene contact engineering for printed electronics. Adv Sci 10(19):e2207174. https://doi.org/10.1002/advs.202207174
18. Li LT, Zhu GX, Wang J et al (2023) A flexible and ultrasensitive interfacial iontronic multisensory sensor with an array of unique "cup-shaped" microcolumns for detecting pressure and temperature. Nano Energy 105:108012. https://doi.org/10.1016/j.nanoen.2022.108012
19. Luo S, Zhou X, Tang XY et al (2021) Microconformal electrode-dielectric integration for flexible ultrasensitive robotic tactile sensing. Nano Energy 80:105580. https://doi.org/10.1016/j.nanoen.2020.105580
20. Yang JC, Kim J, Oh J et al (2019) Microstructured porous pyramid-based ultrahigh sensitive pressure sensor insensitive to strain and temperature. ACS Appl Mater Interfaces 11(21):19472–19480. https://doi.org/10.1021/acsami.9b03261
21. Shen ZR, Yang CD, Yao CJ et al (2023) Capacitive-piezoresistive hybrid flexible pressure sensor based on conductive micropillar arrays with high sensitivity over a wide dynamic range. Mater Horiz 10(2):499–511. https://doi.org/10.1039/d2mh00892k
22. Zhang YJ, Wang YH, Wang CY et al (2023) Superior performances via designed multiple embossments within interfaces for flexible pressure sensors. Chem Eng J 454:139990. https://doi.org/10.1016/j.cej.2022.139990
23. Ji B, Zhou Q, Wu JB et al (2020) Synergistic optimization toward the sensitivity and linearity of flexible pressure sensor via double conductive layer and porous microdome array. ACS Appl Mater Interfaces 12(27):31021–31035. https://doi.org/10.1021/acsami.0c08910
24. Qiao YC, Jian JM, Tang H et al (2022) An intelligent nanomesh-reinforced graphene pressure sensor with an ultra large linear range. J Mater Chem A 10(9):4858–4869. https://doi.org/10.1039/D1TA09813F
25. Chen TJ, Liu ZY, Zhao G et al (2022) Piezoresistive sensor containing lamellar MXene-plant fiber sponge obtained with aqueous MXene ink. ACS Appl Mater Interfaces 14(45):51361–51372. https://doi.org/10.1021/acsami.2c15922
26. Xu T, Song Q, Liu K et al (2023) Nanocellulose-assisted construction of multifunctional MXene-based aerogels with engineering biomimetic texture for pressure sensor and compressible electrode. Nano-Micro Lett 15(1):98. https://doi.org/10.1007/s40820-023-01073-x
27. Song SQ, Zhang CF, Li WZ et al (2022) Bioinspired engineering of gradient and hierarchical architecture into pressure sensors toward high sensitivity within ultra-broad working range. Nano Energy 100:107513. https://doi.org/10.1016/j.nanoen.2022.107513
28. Yang T, Deng WL, Chu X et al (2021) Hierarchically microstructure-bioinspired flexible piezoresistive bioelectronics. ACS Nano 15(7):11555–11563. https://doi.org/10.1021/acsnano.1c01606

29. Wang XM, Tao LQ, Yuan M et al (2021) Sea urchin-like microstructure pressure sensors with an ultra-broad range and high sensitivity. Nat Commun 12(1):1776. https://doi.org/10.1038/s41467-021-21958-y
30. Zhang Y, Yang JL, Hou XY et al (2022) Highly stable flexible pressure sensors with a quasi-homogeneous composition and interlinked interfaces. Nat Commun 13(1):1317. https://doi.org/10.1038/s41467-022-29093-y
31. Liu Y, Xu X, Wei Y et al (2022) Tailoring silver nanowire nanocomposite interfaces to achieve superior stretchability, durability, and stability in transparent conductors. Nano Lett 22(9):3784–3792. https://doi.org/10.1021/acs.nanolett.2c00876
32. Shi XL, Zhu L, Yu H et al (2023) Interfacial click chemistry enabled strong adhesion toward ultra-durable crack-based flexible strain sensors. Adv Funct Mater 33(27):2301036. https://doi.org/10.1002/adfm.202301036
33. Han MM, Shen WH (2022) Nacre-inspired cellulose nanofiber/MXene flexible composite film with mechanical robustness for humidity sensing. Carbohydr Polym 298:120109. https://doi.org/10.1016/j.carbpol.2022.120109
34. Hao SW, Fu QJ, Meng L et al (2022) A biomimetic laminated strategy enabled strain-interference free and durable flexible thermistor electronics. Nat Commun 13(1):6472. https://doi.org/10.1038/s41467-022-34168-x
35. Shi XL, Wang HK, Xie XT et al (2018) Bioinspired ultrasensitive and stretchable MXene-based strain sensor via nacre-mimetic microscale "brick-and-mortar" architecture. ACS Nano 13(1):649–659. https://doi.org/10.1021/acsnano.8b07805
36. Wang LM, Li N, Zhang YF et al (2022) Flexible multiresponse-actuated nacre-like MXene nanocomposite for wearable human-machine interfacing. Matter 5(10):3417–3431. https://doi.org/10.1016/j.matt.2022.06.052
37. Wei J, Jia S, Ma C et al (2023) Nacre-inspired composite film with mechanical robustness for highly efficient actuator powered by humidity gradients. Chem Eng J 451:138565. https://doi.org/10.1016/j.cej.2022.138565
38. Liu H, Chen XY, Zheng YJ et al (2021) Lightweight, superelastic, and hydrophobic polyimide nanofiber/MXene composite aerogel for wearable piezoresistive sensor and oil/water separation applications. Adv Funct Mater 31(13):2008006. https://doi.org/10.1002/adfm.202008006
39. Liu SR, Meng Q, Gao YD et al (2023) Monolithically integrated flexible sensing systems with multi-dimensional printable MXene electrodes. J Mater Chem A 11(25):13238–13248. https://doi.org/10.1039/d3ta01261a
40. Su TY, Liu NS, Lei DD et al (2022) Flexible MXene/bacterial cellulose film sound detector based on piezoresistive sensing mechanism. ACS Nano 16(5):8461–8471. https://doi.org/10.1021/acsnano.2c03155
41. Cheng YF, Xie YM, Cao HH et al (2023) High-strength MXene sheets through interlayer hydrogen bonding for self-healing flexible pressure sensor. Chem Eng J 453:139823. https://doi.org/10.1016/j.cej.2022.139823
42. Yin TT, Cheng YF, Hou YX et al (2022) 3D porous structure in MXene/PANI foam for a high-performance flexible pressure sensor. Small 18(48):e2204806. https://doi.org/10.1002/smll.202204806
43. Liu JJ, Yang WJ, Xu Y et al (2022) MXene-based films via scalable fabrication with improved mechanical and antioxidant properties for electromagnetic interference shielding. Compos Commun 31:101112. https://doi.org/10.1016/j.coco.2022.101112
44. Jin XJ, Li LL, Zhao SF et al (2021) Assessment of occlusal force and local gas release using degradable bacterial cellulose/$Ti_3C_2T_x$ MXene bioaerogel for oral healthcare. ACS Nano 15(11):18385–18393. https://doi.org/10.1021/acsnano.1c07891
45. Wang DY, Wang LL, Lou Z et al (2020) Biomimetic, biocompatible and robust silk fibroin-MXene film with stable 3D cross-link structure for flexible pressure sensors. Nano Energy 78:105252. https://doi.org/10.1016/j.nanoen.2020.105252
46. Wang LL, Wang DP, Wang K et al (2021) Biocompatible MXene/chitosan-based flexible bimodal devices for real-time pulse and respiratory rate monitoring. ACS Mater Lett 3(7):921–929. https://doi.org/10.1021/acsmaterialslett.1c00246
47. Su E, Wu FM, Zhao SQ et al (2022) Layered MXene/aramid composite film for a soft and sensitive pressure sensor. ACS Appl Mater Interfaces 14(13):15849–15858. https://doi.org/10.1021/acsami.2c01914
48. Zhang YP, Wang LL, Zhao LJ et al (2021) Flexible self-powered integrated sensing system with 3D periodic ordered black phosphorus@MXene thin-films. Adv Mater 33(22):2007890. https://doi.org/10.1002/adma.202007890
49. Chen SQ, Wang YD, Fei B et al (2022) Development of a flexible and highly sensitive pressure sensor based on an aramid nanofiber-reinforced bacterial cellulose nanocomposite membrane. Chem Eng J 430:131980. https://doi.org/10.1016/j.cej.2021.131980
50. Fu XY, Li JZ, Li DD et al (2022) MXene/ZIF-67/PAN nanofiber film for ultra-sensitive pressure sensors. ACS Appl Mater Interfaces 14(10):12367–12374. https://doi.org/10.1021/acsami.1c24655
51. Sharma S, Chhetry A, Zhang SP et al (2021) Hydrogen-bond-triggered hybrid nanofibrous membrane-based wearable pressure sensor with ultrahigh sensitivity over a broad pressure range. ACS Nano 15(3):4380–4393. https://doi.org/10.1021/acsnano.0c07847
52. Zheng YJ, Yin R, Zhao Y et al (2021) Conductive MXene/cotton fabric based pressure sensor with both high sensitivity and wide sensing range for human motion detection and E-skin. Chem Eng J 420:127720. https://doi.org/10.1016/j.cej.2020.127720
53. Yao DJ, Tang ZH, Zhang L et al (2021) A highly sensitive, foldable and wearable pressure sensor based on MXene-coated airlaid paper for electronic skin. J Mater Chem C 9(37):12642–12649. https://doi.org/10.1039/d1tc02458b
54. Yang ZP, Li HQ, Li CK et al (2022) Conductive and room-temperature self-healable polydimethylsiloxane-based elastomer film with ridge-like microstructure for piezoresistive pressure sensor. Chem Eng J 430:133103. https://doi.org/10.1016/j.cej.2021.133103
55. Chao MY, He LZ, Gong M et al (2021) Breathable $Ti_3C_2T_x$ MXene/protein nanocomposites for ultrasensitive medical pressure sensor with degradability in solvents. ACS Nano 15(6):9746–9758. https://doi.org/10.1021/acsnano.1c00472